analytical chemistry

pubs.acs.org/ac Article

Influence of Chemical and Genetic Manipulations on Cellular Organelles Quantified by Label-Free Optical Diffraction Tomography

Min Ju Cho,[‖] Chae-Eun Kim,[‖] Yeon Hui Shin, Jun Ki Kim,* and Chan-Gi Pack*

Cite This: *Anal. Chem.* 2023, 95, 13478−13487 Read Online

ACCESS | Metrics & More | Article Recommendations | Supporting Information

ABSTRACT: Label-free optical diffraction tomography provides three-dimensional imaging of cells and organelles, along with their refractive index (RI) and volume. These physical parameters are valuable for quantitative and accurate analysis of the subcellular microenvironment and its connections to intracellular biological properties. In biological and biochemical cell analysis, various invasive cell manipulations are used, such as temperature change, chemical fixation, live cell staining with fluorescent dye, and gene overexpression of exogenous proteins. However, it is not fully understood how these various manipulations affect the physicochemical properties of different organelles. In this study, we investigated the impact of these manipulations on the cellular properties of single HeLa cells. We found that after cell fixation and an increase in temperature, the RI value of organelles, such as the nucleus and cytoplasm, significantly decreased overall. Interestingly, unlike the cell nuclei, cytoplasmic RI values were hardly detected after membrane permeation, indicating that only intracytoplasmic components were largely lost. Additionally, our findings revealed that the expression of GFP and GFP-tagged proteins significantly increased the RI values of organelles in living cells compared to the less effective RI changes observed with chemical fluorescence staining for cell organelles. The result demonstrates that distinct types of invasive manipulations can alter the microenvironment of organelles in different ways. Our study sheds new light on how chemical and genetic manipulations affect organelles.

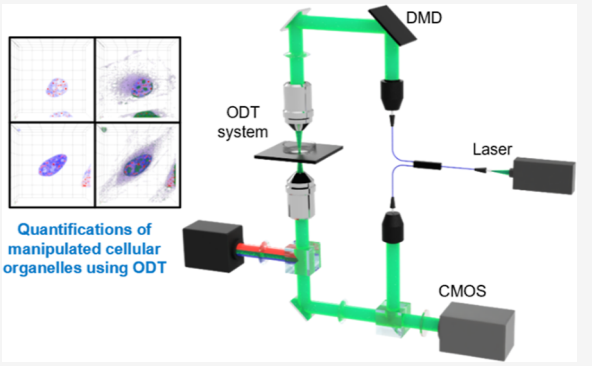

INTRODUCTION

Cellular organelles and biomolecules in live cells are well organized spatiotemporally within a limited volume to express the biological functions of cells through dynamic changes in their properties. As a result, even cells of the same type show changes in biological and physical properties under various physiological conditions. In biological experiments, cells are often stimulated by various treatments, such as cytokines, drugs, and environmental stress, for cell function analysis. Afterward, changes in intracellular reporter genes, such as the presence or absence of expression and expression intensity, or morphological changes of organelles are observed through various invasive processes, including cell imaging techniques and conventional biochemical methods like immunoprecipitation and immunoblotting. With the advancement of cell imaging technology, low- and high-resolution fluorescence microscopy has been often used for the analysis of reporter genes, and electron microscopy has been also used to detect ultra-structure morphological changes in organelles.[1] For these microscopic assays, fixed cells are often used. In cell biology and biophysical studies, specific molecules or organelles in live cells are imaged and analyzed through advanced fluorescence techniques such as high-resolution laser scanning confocal microscopy, single molecule detection, and fluorescence correlation spectroscopy to obtain biological and biophysical information, such as subcellular distribution and kinetic properties, of the target molecule (organelle).[2−4] All of these microscopic imaging and analytical techniques require a cell preparation process, such as chemical cell fixation, ultra-sectioning, and fluorescence staining. Unlike electron microscopy, fluorescence methods allow direct observation of living cells without chemical fixation, although a pre-treatment process of fluorescence labeling for specific molecules or organelles is required. While these microscopic methods are very useful for high-resolution observation of changes in the characteristics of the molecule or organelle which cause variations in the physiological conditions of cells, they have limitations in that they involve invasive manipulations of the cells.

Received: March 29, 2023
Accepted: July 21, 2023
Published: July 31, 2023

Downloaded via UNIV OF ULSAN COLG OF MEDICINE on September 13, 2023 at 00:49:52 (UTC).
See https://pubs.acs.org/sharingguidelines for options on how to legitimately share published articles.

ACS Publications © 2023 American Chemical Society

https://doi.org/10.1021/acs.analchem.3c01349
Anal. Chem. 2023, 95, 13478−13487

Label-free optical diffraction tomography (ODT) is a quantitative phase imaging technique that combines two-dimensional (2D) holograms obtained from various angles to reconstruct three-dimensional (3D) images of cells and organelles.[5] Unlike other techniques, ODT does not require a pre-process for cell observation, even for living cells.[6−8] The 3D image reconstructed by ODT provides quantitative information on refractive index (RI) and volume, making it useful for assessing changes in the physical properties of cells due to physiological conditions or artificial manipulation.[9−15] A change in the RI value, which is a physical parameter presented as an absolute value in cells, can also be a measure of intracellular biological changes since the RI is proportional to the density of molecules.[16] However, label-free ODT based on intracellular differences in RI has limited access to specific molecular information. To address this limitation, a method combining fluorescence microscopy and RI tomography has recently been developed.[17−19] This technique provides molecular-specific information and physicochemical information about cells or organelles and can be applied to various studies using living cells and fixed cells.

Practically, fluorescent imaging requires various manipulations, such as chemical fixation and permeabilization of cells, for immunostaining or gene expression into living cells by transfection reagents for fluorescent labeling of target molecules. As a result, cells undergo various chemical and genetic invasions, depending on the manipulation. Alternatively, specific organelles such as the plasma membrane (PM), mitochondria, lysosome, and endoplasmic reticulum (ER) can be directly stained by a fluorescent organic dye known as an organelle tracker, and then, the stained live cells are analyzed under fluorescence microscopy.[20] These trackers are membrane-permeable dyes and are therefore considered relatively less invasive to cells. Studies using ODT have analyzed the RIs of living cells and fixed cells and suggested that the RI of compartments or organelles decreased when cells were fixed by paraformaldehyde (PFA), and the observed RI changes vary between different cell lines.[21,22] Additionally, the mechanical properties of the cell surface and cellular nanostructure after chemical fixation have been analyzed by atomic force microscopy and particle-wave spectroscopic microscopy, respectively.[23,24] Nevertheless, it is still unclear how various cell manipulations including chemical fixation affect cells or organelles.

In this study, we present an analytical technique that uses label-free ODT and fluorescence-correlated ODT to quantitatively evaluate the effects of cellular manipulations on organelles in single cells. To evaluate the influence, organelles were divided into cell PM, nucleolus, cytoplasm/nucleoplasm, and perinuclear ER regions. The absolute RI value of organelles is considered a crucial parameter in representing the characteristics of individual cells; therefore, we demonstrated RI measurements of the four cellular organelles after temperature change, chemical cell fixation, and membrane permeabilization for immunofluorescence. Moreover, we evaluated the RI value of the organelles after live cell fluorescent labeling through the genetic expression of GFP tagging proteins or the use of fluorescent organelle trackers. Our approach aims to deepen our understanding of the impact of various invasive manipulations on the physicochemical properties of individual cells at the subcellular level and to improve the reliability of molecule- and organelle-targeted fluorescent probes for various cell imaging methods.

EXPERIMENTAL SECTION

Cell Culture and Fixation. HeLa cells were cultured in Dulbecco's modified Eagle medium (DMEM) supplemented with 10% fetal bovine serum (FBS), 100 U/mL penicillin, and 100 U/mL streptomycin at 37 °C in a 5% CO_2 incubator. HeLa cells were plated and cultured in Tomo-dishes with a microscope cover glass (Tomocube, Daejeon, Korea) for ODT observation or a combination of ODT and fluorescence imaging. HeLa cells were divided into live, fixed cell, immunofluorescence staining, and gene transfection categories. Label-free live cells were observed under two different temperature conditions: 25 and 37 °C in Dulbecco's phosphate-buffered saline (PBS) (Biowest, Nuaille, France). In the case of fixed cells, HeLa cells were fixed in 4% PFA (T&I, Chuncheon, Korea) in 0.1 M PBS, washed with PBS, and observed in PBS at 25 °C.[25,26] HeLa cells stably expressing GFP-LC3 were generously donated by Dr. T. Yoshimori from Osaka University, Osaka, Japan.[27]

Immunofluorescence Staining. HSF4 monoclonal antibody (Invitrogen, Oregon, USA, 1:300 dilution) and nucleophosmin (Abcam, Cambridge, UK, 1:200 dilution), also known as nucleolar phosphoprotein B23, served as primary antibodies. Alexa flour 488 (Life Technologies, California, USA) was used as the secondary antibody for fluorescence. Sodium citrate buffer of 0.01 M (pH 6.0) was used for washing, and 0.1% Triton X-100 and 0.05% Tween 20 in sodium citrate buffer were used for antigen retrieval.[28,29] DAPI (Invitrogen, Oregon, USA, 1:1000 dilution) was used for counterstaining. Cells were washed with PBS buffer during the immunofluorescence staining process.

Fluorescent Dyeing of Organelles for Live Cell Imaging. To observe each cellular organelle in single live cells, HeLa cells were prepared and observed with various cell organelle trackers, such as nuclear staining reagent Hoechst 33342 (NucBlue Live ReadyProbes Reagent, Invitrogen, Carlsbad, USA, 1 drop/mL), MitoTracker Deep Red FM (Invitrogen, Carlsbad, USA, 1:5000 dilution), ER-Tracker Blue-White DPX (Invitrogen, Carlsbad, USA, 1:2000 dilution), LysoTracker Red DND-99 (Invitrogen, Carlsbad, USA, 1:300 dilution), and lipid droplet-tracker (LD-tracker) of Lipid-Spot488 Lipid Droplet Stain (Biotium, Fremont, USA, 1:1000 dilution). Live cell staining of the trackers was performed according to the manufacturers' optimized protocols.

Plasmids. Plasmids expressing monomeric RFP-B23 (nucleophosmin) fusion protein (mRFP-B23), GFP-Lamin A fusion protein (GFP-LA), EGFR-GFP fusion protein (EGFR-GFP), and monomeric GFP (GFP) were described in a previous study.[2,4,12,30−32] The plasmid constructs were verified through sequencing. Purification of the plasmid constructs used for transfection was done using a plasmid DNA Midiprep kit (Qiagen, Hilden, Germany).

Cell Transfection. For transient expression of GFP or GFP-tagged proteins, cultured HeLa cells were seeded in Tomo-dishes (Tomocube, Daejeon, Korea). Gene-specific expression in HeLa cells was induced using Lipofectamine 3000 Transfection Reagent (Thermo Fisher Scientific, Waltham, Massachusetts) according to the manufacturers' optimized protocols. Fluorescence observation was performed 24 h after transfection.

Label-Free ODT and Correlative Fluorescence Imaging with RI Tomography. Label-free ODT was performed as described previously.[7,13,33] ODT uses 3D RI tomography to

https://doi.org/10.1021/acs.analchem.3c01349
Anal. Chem. 2023, 95, 13478−13487

reconstruct a single HeLa cell from multiple 2D holograms taken from various angles.[34] The ODT measurements of single living cells were performed using a commercial ODT microscope (HT-2H, Tomocube Inc., Daejeon, Korea) under a 5% CO_2 atmosphere at 25 or 37 °C using a 532 nm laser light source [10; 32; 7]. The commercial ODT microscope, which includes a Mach−Zehnder interferometer microscope, was used to reconstruct the 3D RI tomography of cells. The ODT microscope also contains an optical unit for 2D or 3D fluorescence imaging of the sample cell with three channels of RGB color. Details of the optical setup for the ODT and fluorescence imaging system are described in Figure S1. In brief, the microscope was composed of a light source/sample modulation device and an optical field detector device. Optical interference was used to record the amplitude and phase information from light passing through a cell sample. Adjustment of the power and exposure time of the laser projected onto the sample cells was first performed to ensure that it did not negatively affect the RI value measurement or image quality; these parameters were then fixed during the ODT or correlative fluorescence imaging measurement. To verify the capability and reliability of the system, fluorescent microspheres with a known RI value and diameter of 5.64 or 6.1 μm (Polysciences Inc., Warrington, USA) were used.[13,35] The lateral and axial optical resolutions of the ODT system were 110 and 365 nm, respectively. The resolution of the RI value is <0.0001 (33; 8). All the 2D or 3D fluorescent images of HeLa cells were obtained using the ODT instrument in combination with fluorescence microscopy. Hoechst 33342 and ER-tracker were excited through an excitation filter of 392 ± 12 nm, and fluorescence was detected by a band-path filter of 432 ± 18 nm. GFP and LD-tracker were excited through excitation filters of 474 ± 14 nm and detected by band-path filters of 523 ± 23 nm. RFP, MitoTracker, and LysoTracker were excited through excitation filters of 575 ± 12 nm and detected by band-path filters of 702 ± 98 nm. The RI values of the culture media of DMEM, PBS, and distilled water at different temperatures were measured using a refractometer (Abbemat 3200; Anton Paar GmbH, Graz, Austria) and used as the reference RI value for each ODT measurement.

Image Rendering and Evaluation of the RI. The RI isosurface of various cellular organelles, such as the PM, cytosol/nucleus, nuclear envelope, nucleolus, lipid droplets, and other high-intensity regions around the nucleus, was rendered using TomoStudio software (Tomocube Inc., Daejeon, Korea), following the manufacturer's protocol.[13,35] The software was also used to calculate the RI values within the rendered image. The transfer functions, representing various RI values and the range of the RI gradient sizes, were altered using TomoStudio's virtual palette until 3D-rendered images of each organelle were adequately represented compared to the reference or the correlative fluorescence image. The median value of the RI range used for image rendering was used to calculate the mean RI values for various organelles and partial regions of single HeLa cells in each media condition.

Statistical Methods. Student's *t*-tests were performed to compare the mean values and determine significance (Origin v.8.5; USA). All *P*-values <0.05 were considered significant.

RESULTS AND DISCUSSION

Acquisition and Evaluation of the ODT Image of Label-Free Cells or Fluorescently Labeled Cells. Acquisition and evaluation of ODT images of label-free cells or fluorescently labeled cells. The optical setup and information regarding the ODT instrument combined with fluorescence microscopy used in this study are presented in Figure S1. The label-free measurement of cells was performed by acquiring multiple 2D holograms of a HeLa cell at various illumination angles via a Mach−Zehnder interferometric microscope equipped with a digital micromirror device. The scattered light from the transparent cell interfered with the tile reference light and generated a spatially modulated hologram (Figure S1). Phase images were obtained from the recorded holograms and amplitudes of the cell using a phase search algorithm.[36,37] Based on the algorithm, ODT produces an RI distribution by assembling the RI range of images acquired from 2D holograms. 3D RI tomography of the sample was reconstructed from several 2D hologram images, as shown in Figure S1. There are several methods for fluorescent labeling of cells in the field of cell biology, which can be broadly categorized into three types. First, to detect the distribution of a target protein in cells through immunostaining, cells need to be chemically fixed and their membrane permeated. Second, for observing the distribution of a target protein in real time in living cells, a genetic method of expressing a GFP-tagged target protein is employed. Lastly, to observe the real-time behavior of living cells, organelles such as nuclear DNA, mitochondria, lysosomes, (ER), and lipid droplets can be fluorescently stained using organic dyes (i.e., fluorescence trackers). The second and third methods are often used in conjunction. ODT measurement is performed on fluorescently labeled cells to obtain 2D- or 3D fluorescence images within seconds. 3D fluorescence images are typically acquired by scanning the objective lens along the *Z*-axis separately from the ODT system. The RI-rendered image of ODT and the fluorescence image of a fluorescently labeled HeLa cell obtained sequentially in this way can be analyzed as correlative ODT and fluorescence images (Figure S1). Previous studies have suggested that the nucleolus has a heterogeneous structure expressed by three RI values and that the PM, cytoplasm, and nucleoplasm can be analyzed separately using different RI values.[12,15] For clarity and simplicity, this study examined whether HeLa cells could be divided into four different regions based on their RI range: cell PM, nucleolus surrounded by the nuclear envelope (NO), cytosol (Cyt), and dense perinuclear region, where the ER and mitochondria overlap (PNER). For this purpose, cells were stained with fluorescent probes that targeted each organelle and compared to organelles analyzed by the RI. RI profiles agreed well with the fluorescence intensity profiles of the fluorescent probes (Figures S1 and S2). Based on the classification of the four regions (i.e., organelles) with different RI values, we compared the mean RI values (i.e., mean molecular density) of each organelle before and after various cell manipulations. There is a difference of a few seconds from the acquisition of the ODT image to that of the fluorescence image, but it was assumed that each organelle does not move significantly compared to the size of cells and organelles. However, lysosomes or lipid droplets, which are thought to be small in size and move quickly, may cause a positional difference between the ODT and fluorescence image in the correlative image even for a short time of several seconds.[38,39] Despite this, it is worth noting that the correlative ODT and fluorescence image is useful for determining whether cells are properly stained based on the method used and for comparing the fluorescence images of each labeled organelle and GFP-tagged proteins with the RI-rendered images.

https://doi.org/10.1021/acs.analchem.3c01349
Anal. Chem. 2023, 95, 13478−13487

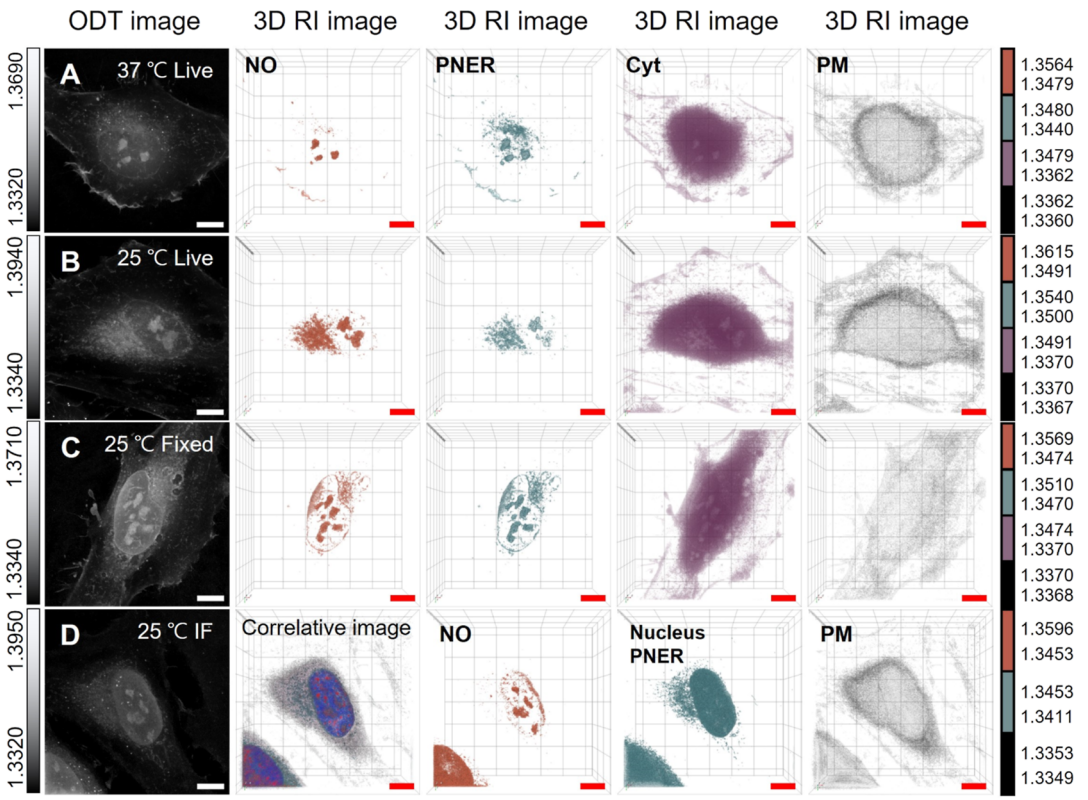

Figure 1. Representative ODT- and RI-rendered images of HeLa cells in PBS buffer at 37 (A) and 25 °C (B), cell fixation by 4% PFA (C), and cell permeabilization by 0.1% Triton X-100 followed by immunofluorescence staining (D). The permeabilized cell was doubly immunostained by Hoechst (blue) and HSF4 (red). For the RI-rendered image of (D), a 2D correlative fluorescence image is also shown (FL + RI). The RI ranges used for RI rendering are depicted by pseudo-color bars. NO, PNER, Cyt, PM, FL, and RI stand for the nucleolus, perinuclear ER region, cytoplasm, PM, fluorescence, and RI, respectively. Scale bars, 10 μm.

Influence of Temperature, Chemical Fixation, and Cell Permeabilization on Organelles. In previous studies, the effects of chemical fixation on the physical properties of cells were investigated.[21−24] However, manipulations such as fluorescence staining of antibodies after permeabilization of cell membranes are often used in addition to cell fixation.[40] Fluorescent imaging of target molecules in living and fixed cells or high-sensitivity analysis methods are often performed at a room temperature of 25 °C instead of the cell culture temperature of 37 °C to avoid problems such as mechanical vibration or draft of the microscopic device. However, it is still unclear whether these temperature differences affect the actual organelles differently. We investigated the influence of temperature change from 37 to 25 °C, chemical fixation by 4% PFA, and cell permeabilization by 0.1% Triton X-100 on the four cellular regions of single HeLa cells (Figure 1). Although the morphology of the cells measured at room temperature by ODT did not show a significant difference in morphology from those measured at the cell culture temperature, it was found that the RI of each organelle increased as the temperature decreased by 12° (Figure 1A,B). Practically, the RI of media solutions is linearly proportional to temperature (Figure S3; Table S1).[35,41,42] As the temperature decreased, the RI value of the PBS solution increased by 0.0015, whereas the RI values of the two organelles NO and PNER increased significantly more than the solution, by 0.0034 and 0.0029, respectively. On the other hand, the RI values of the two organelles, Cyt and PM, showed a similar increase to that of the PBS solution at 0.0014 and 0.0011, respectively. This result suggests that the high-density organelles, which are heterogeneous systems, change more sensitively to temperature than the solutions, which are open and homogeneous systems. Unlike the cell membrane or cytoplasm, the NO and PNER are densely packed with high-density proteins and RNA molecules and play a role in maintaining cell homeostasis. Therefore, it seems that the function is expressed through active density change in order to relieve the stress of temperature change. Compared to living cells at room temperature, the RI values of the three organelles of chemically fixed cells were found to decrease even without apparent morphological change (Figure 1B,C). The decrease in the RI of organelles by chemical fixation is in good agreement with the results of a previous study.[22] In another previous study, swelling of HeLa cells by PFA fixation has been reported, and such swelling of HeLa cells may cause a decrease in the RI value of the organelles.[21] It is likely that PFA fixation caused this swelling (increase in intracellular water or solvent) by consequently changing the permeability of intracellular and extracellular molecules. We subsequently investigated the influence of a typical permeabilization detergent, 0.1% Triton X-100, and antibody immunostaining on cellular organelles (Figure 1D and Supporting Information Movie S1). Surprisingly, cell permeabilization significantly reduced the overall intracellular density, including the PM. Especially, it could not be detected compared to the other three organelles of the nucleolus, nucleoplasm, and PNER, suggesting that more soluble macromolecules from the cytoplasm were released from the cell. Morphologically, compared to living cells or fixed

https://doi.org/10.1021/acs.analchem.3c01349
Anal. Chem. 2023, 95, 13478−13487

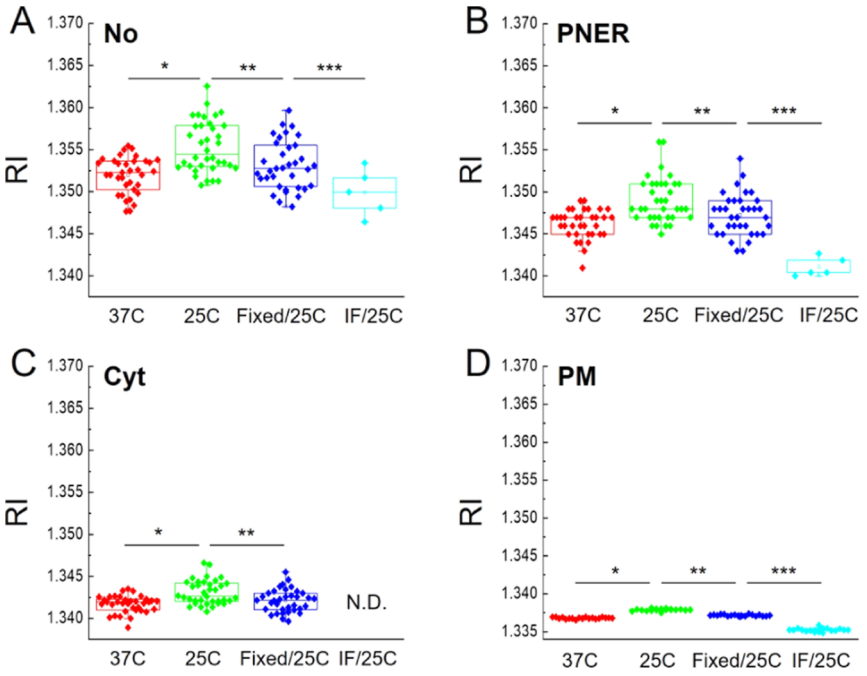

Figure 2. Summarized RI values of organelles of HeLa cells in PBS buffer according to temperature change and cell manipulations. The temperature was changed from 37 to 25 °C. Cells were fixed with 4% PFA and measured at 25 °C (fixed/25 °C). Immunofluorescence staining was performed after cell permeabilization by 0.1% Triton X-100 and measured at 25 °C (IF/25 °C). Averaged RI values of the nucleolus (NO) surrounded by the nuclear membrane (A), the dense perinuclear region where the ER and mitochondria overlap (PNER) (B), the cytosol (Cyt) (C), and the cell PM (D) are shown, respectively. N.D. means no detection. *, **, and ***$P < 0.05$ (Student's *t*-test).

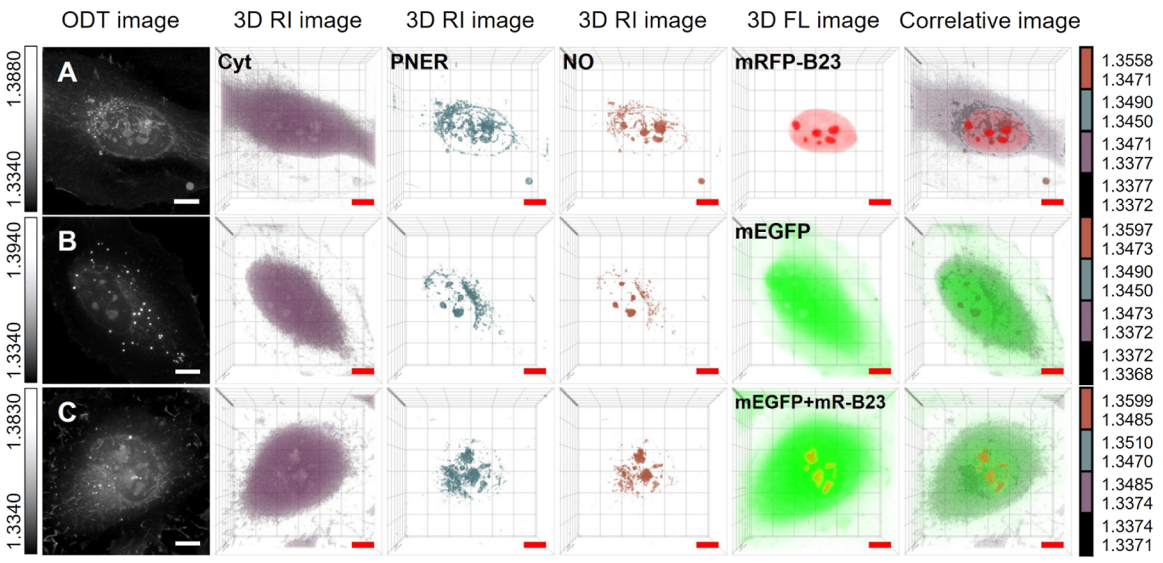

Figure 3. Representative ODT- and RI-rendered images of live HeLa cells transiently expressing GFP-tagged proteins. Live HeLa cells overexpressing mRFP-B23 (A), mEGFP (B), and overexpressing mRFP-B23 in addition to mEGFP (C) are shown. All cells were measured after 24 h in fresh DMEM by ODT (see also the Experimental Section). For the RI-rendered images from (A) to (C), the 3D correlative fluorescence images are also shown. The RI ranges used for RI rendering are depicted by pseudo-color bars. NO, PNER, and Cyt denote the nucleolus, perinuclear ER region, and cytosol, respectively. Scale bars, 10 μm.

cells, the PNER of the immunostained cell after permeabilization showed a significantly large and prominent shape (see also Figure S4). This is likely to have occurred because the contrast of the PNER was increased by the large decrease of the RI in the cytosol. To obtain a more detailed understanding of the properties of the nucleus and nucleolus, we performed immunostaining for DNA, HSF4 (heat shock transcription factor 4), and nucleolar protein B23 to confirm the normal distribution of nuclear proteins. As a result of immunostaining for HSF4 and B23, which are known to be localized in the nucleoplasm and nucleolus, respectively,[43−45] it was confirmed that these nuclear and nucleolar proteins are well-preserved in their respective locations, despite the overall decrease in RI value in the nucleus and the morphological change of the nucleolus (Figures 1D and S4). Figure 2 summarizes the influence of temperature change, chemical fixation, and transmembrane manipulation on the mean RI value of the four intracellular organelles. The result demonstrates that

https://doi.org/10.1021/acs.analchem.3c01349
Anal. Chem. 2023, 95, 13478−13487

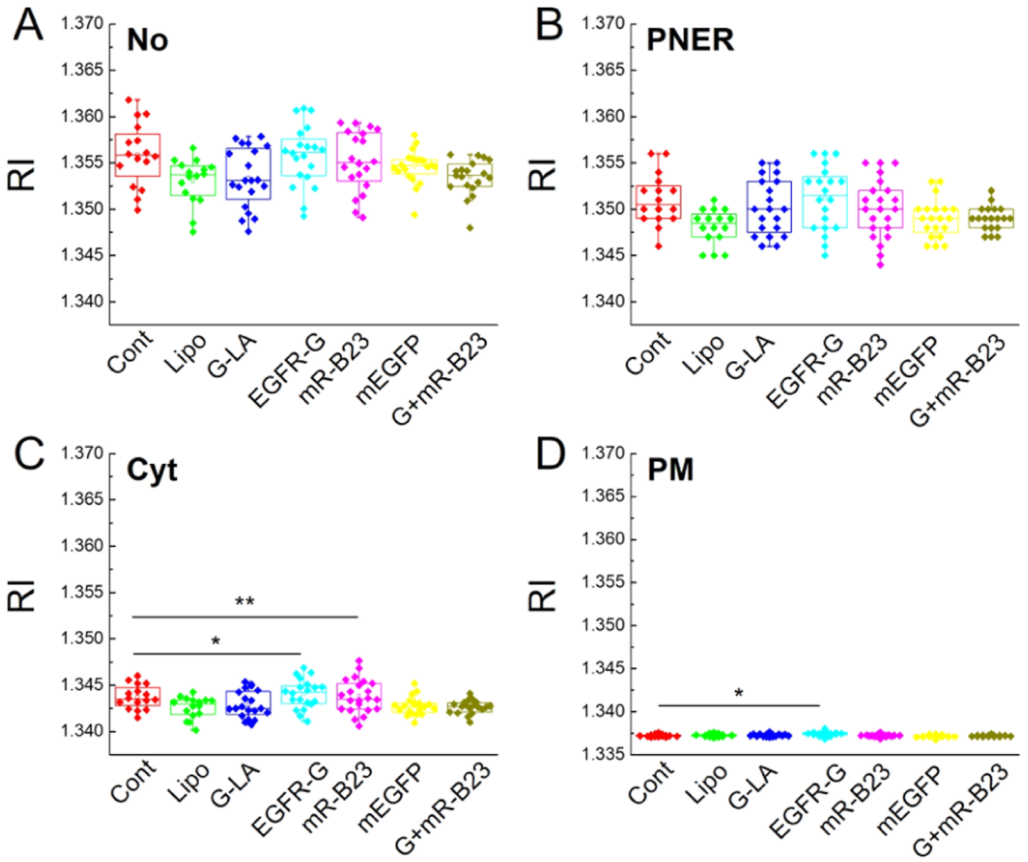

Figure 4. Summarized RI values of four cellular organelles of normal and transfected HeLa cells. All HeLa cells were analyzed in DMEM complemented with 10% FBS at 37 °C. Averaged RI values of the nucleolus surrounded by the nuclear membrane (NO) (A), the dense perinuclear region where the ER and mitochondria overlap (PNER) (B), the cytoplasm (Cyt) (C), and the cell PM (D) are shown, respectively. Cont, Lipo, G-LA, EGFR-G, mR-B23, mEGFP, and G + mR-B23 stand for cells without manipulation, transfected cells with lipofectamine 3000, cells expressing GFP-Lamin A, EGFR-GFP, mRFP-B23, mEGFP, and cells co-expressing GFP and mRFP-B23, respectively. * and **$P < 0.05$ (Student's *t*-test).

temperature change and chemical cell fixation induce homogeneous changes of RI in organelles, while cell permeabilization has a large and much distinct effect on organelles, especially on the cytosol. A previous study using surface plasmon resonance imaging techniques found that permeabilization by Triton X-100 eliminated much more cellular membrane lipids and significantly reduced intracellular mass density.[40] Our results, which suggest a large loss of intracellular cytosolic components and a large decrease in the overall RI of cells caused by permeabilization, are in good agreement with the results of this previous study obtained by surface plasmon resonance analysis. The present and previous findings collectively suggest that, unlike PFA fixation, permeabilization acts on the extracellular release of large amounts of intracellular macromolecules.

Evaluation of the Influence of Transient Gene Overexpression on Single HeLa Cells. Recently, in cell biology, microscopic imaging technologies have been widely used to genetically combine fluorescent proteins of various colors with target proteins and express them in single living cells. This is done to analyze the intracellular distribution or dynamic characteristics of target proteins. The genetic cell manipulation requires intracellular delivery of target genes using a transfection reagent of cationic liposomes, and the expression of the transfected genes can be detected within 12 to 42 h[46,47] Despite the various transfection methods that have been developed,[48] the full impact of these transfection and gene overexpression processes on the physiochemical properties of organelles is not yet understood. We investigated the effect of genetic overexpression of various fluorescent protein-tagged proteins after transient transfection using cationic liposomes on the RI of intracellular organelles (Figures 3, S5). To investigate the effect of monomeric GFP or monomeric RFP-tagged proteins with different intracellular localizations on organelles, first, the effect of transfection itself on HeLa cells was evaluated by comparing cells subjected to transfection using the reagent cationic liposome with cells without manipulation (Figure S5). Next, ODT measurements were performed by selecting Lamin A (GFP-LA) localized in the nuclear membrane and nucleoplasm,[49] epidermal growth factor receptor (EGFR-GFP) localized in the PM and perinuclear ER regions, respectively (Figure S5).[32] Additionally, we investigated HeLa cells expressing nucleophosmin B23 (mRFP-B23) localized in the nucleolus.[4,30] We also examined cells expressing only monomeric GFP (mGFP), which has no biological function, and cells that co-express mGFP and mRFP-B23 together (Figure 3A–C).[2,4] No morphological changes in the whole cell were detected in all conditions. Although the shape of the nucleolus is often round (Figures 3, S5), it is unclear whether the effect was due to transfection or overexpression of GFP-tagged proteins because there were cells in which the nucleolus was round even under normal conditions without transfection. The intracellular fluorescence distributions of GFP-LA, EGFR-GFP, mRFP-B23, and GFP

https://doi.org/10.1021/acs.analchem.3c01349
Anal. Chem. 2023, 95, 13478−13487

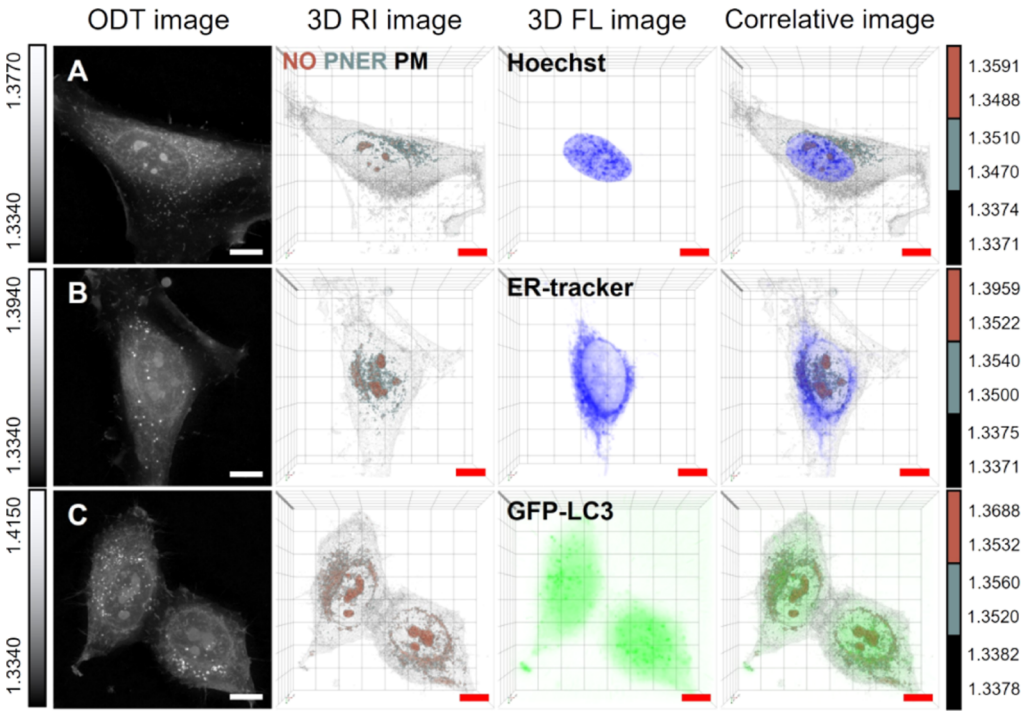

Figure 5. Comparison of live HeLa cells stained by fluorescent trackers with cells stably expressing GFP-LC3. Representative ODT-, RI-rendered, and fluorescence images of live HeLa cells stained by DNA-Tracker (Hoechst) (A) and ER-tracker (B) are shown. (C) Representative ODT-, RI-rendered, and fluorescence images of live HeLa cells stably expressing GFP-LC3. The RI ranges used for RI-rendered images are depicted by pseudo-color bars. NO, PNER, and PM represent the nucleolus, perinuclear ER region, and PM, respectively. Scale bars, 10 μm.

proteins were consistent with previous studies.[2,4,49,50] For the GFP/mRFP-tagged proteins localized in each specific organelle, the region of strong fluorescence intensity of the proteins for each organelle is well aligned with the region of high RI of the corresponding organelle. For cells expressing EGFR-GFP, a high RI was detected in the region, where the fluorescence intensity of EGFR-GFP was high in the cell membrane and PNER (Figure S5). When analyzing the RI specifically in the PM, it was found that the RI of the PM of cells expressing EGFR-GFP was much higher compared to cells without expression (Figure S6). However, regions adjacent to the PM with high RI are often present, even in normal cells without overexpression of EGFR-GFP, making it difficult to consider it an increase in RI due to the overexpression (Figure S5). This suggests that EGFR-GFP is predominantly distributed in the PM or a specific region of high density adjacent to the PM. Figure 4 summarizes the effect of transfection manipulation and overexpression of GFP/mRFP-tagged proteins on the mean RI value of the four intracellular organelles. No significant RI changes were detected in the nucleolus or PNER by overexpression of GFP or GFP-tagged proteins. However, it was found that the RI of the cytosol was significantly increased in cells overexpressing EGFR-GFP or mRFP-B23, and the RI of the PM only increased significantly in cells overexpressing EGFR-GFP.

Influence of Cell-Permeable Fluorescent Trackers and Stable Expression of GFP-Tagged LC3 on HeLa Cells. In addition to the genetic method for transient expression of GFP-tagged proteins, easy methods of fluorescently staining specific organelles of living cells using organic dyes have been commonly used in cell biological experiments. Various organic dyes, also known as fluorescent trackers, are capable of specifically staining different organelles, including Hoechst for nuclear DNA staining, ER-tracker for ER, MitoTracker for mitochondria, LysoTracker for lysosomes, and LD-tracker for lipid droplets.[51−53] We analyzed the influence of these five fluorescence trackers on the physical properties of each organelle (Figures 5A,B and S7). Furthermore, the physical characteristics of HeLa cells stably expressing GFP-LC3 were compared to the results obtained from these fluorescent trackers (Figure 5C). Unlike transient transfection using cation liposomes, cells stably expressing fluorescent proteins are analyzed in a state where the physicochemical stimulation (i.e., transfection by reagent) to cells is minimized, and thus, they were compared to the membrane-permeable trackers, which also minimize the external stimulation. HeLa cells stably expressing GFP-LC3, a maker protein of the autophagosome, are widely used in autophagy research.[54−56] No significant morphologic changes were observed in the cells treated with each fluorescent tracker. As shown in Figures 5 and S7, each fluorescent tracker represents the distribution of organelles based on the fluorescence intensity. Among them, ER-tracker and MitoTracker show high fluorescence mainly in the PNER together, indicating that the dense ER and mitochondria are intermingled in that region. Although it is unclear which of the two organelles contributes more to the high density of PNER domains, the results support the formation of a PNER with a high RI, as detected in ODT (see also Figure S1). Although mitochondria are also found in the PNER, their discontinuous and thin linear structure contributes less to the high-density structure compared to the continuous and sheet structure of the rough ER.[57,58] The fluorescence of the LysoTracker was distributed throughout the cytoplasm and showed a granular structure with a non-uniform size (Figure S7). In contrast, the fluorescence of the LD-tracker was

https://doi.org/10.1021/acs.analchem.3c01349
Anal. Chem. 2023, 95, 13478−13487

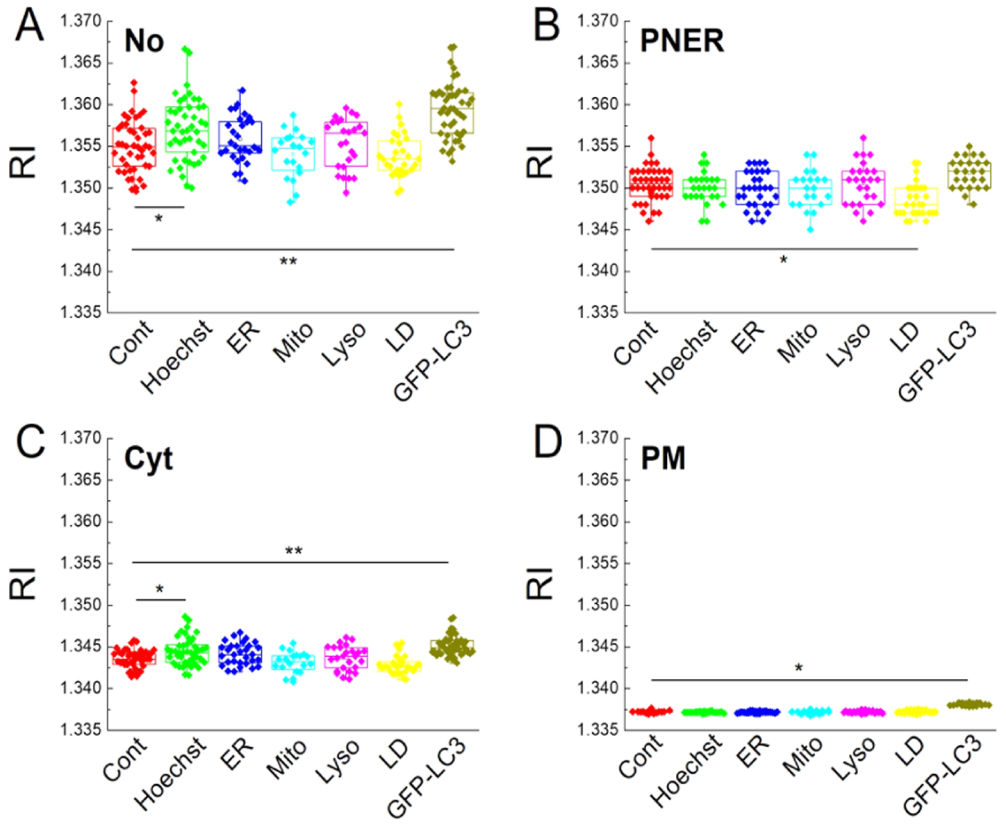

Figure 6. Summarized RI values of four cellular organelles of normal cells, cells after fluorescence staining, and cells stably expressing GFP-LC3. All live HeLa cells were analyzed in DMEM complemented with 10% FBS at 37 °C. Averaged RI values of the nucleolus surrounded by the nuclear membrane (NO) (A), the dense perinuclear region where the ER and mitochondria overlap (PNER) (B), the cytoplasm (Cyt) (C), and the cell PM (D) are shown, respectively. * and **$P < 0.05$ (Student's *t*-test).

predominantly located in the PNER and displayed a circular grain structure with a relatively uniform size (Figure S7).

Structures with high RI colocalizing with fluorescence of LysoTracker were unclear, while structures (i.e., lipid droplets) with high RI colocalizing with fluorescence of LD-tracker were clearly detected. In previous studies using ODT without correlative fluorescence, it was demonstrated that lipid droplets were easily detected because of their circular shape, with a uniform volume of 0.47 μm^3 on average and a much higher RI of ~1.385 on average compared to other organelles.[12,59] Our results, which combined ODT with fluorescence microscopy, are in good agreement with those of previous studies. HeLa cells stably expressing GFP-LC3 had a smaller cell size compared to cells under other conditions, but the PNER was dense and widely expanded toward the cytoplasm (Figure 5C). The RI of each organelle was found to be relatively higher than that of normal cells. The fluorescence of GFP-LC3 is evenly distributed in the cytoplasm and nucleus at normal conditions, which is consistent with previous studies.[56,60]

Figure 6 summarizes the influence of chemical fluorescence staining on live cells and stable overexpression of GFP-LC3 on the mean RI value of the four intracellular organelles. In HeLa cells stained with Hoechst, the RI of nucleoli and cytosol was significantly higher than that of normal HeLa cells, and no significant changes were detected in the rest of the organelles. In contrast, the RI detected in the PNER area of cells stained with LD-tracker was lower compared to normal cells. The RI of each organelle in cells stained with ER-, Mito, and LysoTracker was not significantly different from that of normal cells. Finally, HeLa cells stably expressing GFP-LC3 showed a significant increase in RI in all organelles except the PNER. This result suggests that the method of stably expressing a GFP-tagged protein significantly changes the physicochemical properties of cells and organelles compared to the method of overexpressing a GFP-tagged protein transiently or chemically fluorescently modifying organelles.

CONCLUSIONS

In summary, we used label-free ODT in conjunction with correlative ODT and fluorescence microscopy to quantitatively evaluate the impact of conventional invasive cell manipulations on the molecular density of intracellular organelles in single HeLa cells. We demonstrated that ODT can provide a three-dimensional distribution of various organelles or distinct regions with different densities. Temperature elevation and cell fixation resulted in decreased organelle density. Surprisingly, cell membrane permeabilization for immunofluorescent staining resulted in a significant loss of various components within each organelle. In particular, there was a substantial loss of components in the cytosol to the extent that the RI was undetectable. Additionally, the effect of genetic cell manipulation and chemical fluorescence staining of live HeLa cells was also investigated. Genetic overexpression of GFP or GFP-tagged proteins using reagent transfection increased organelle density, depending on the type of tagged protein. Interestingly, it was found that the cells in which the protein was stably overexpressed showed significant changes in cell volume and density. Conversely, the fluorescence trackers used for fluorescence staining of specific organelles did not significantly

https://doi.org/10.1021/acs.analchem.3c01349
Anal. Chem. 2023, 95, 13478−13487

affect organelle density. Therefore, various chemical reagents and experimental techniques, such as gene transformation, used in biological experiments can induce physical changes in cells compared to organelle trackers. Consequently, when performing biological and biochemical analysis of organelles combined with fluorescence microscopy or ODT using invasive cell manipulations, it is necessary to consider changes in the properties of organelles that may occur depending on each treatment condition. Our study provides valuable information for the development of less invasive cell manipulation methods and the design of organelle-targeted fluorescent probes for reliable and non-invasive intracellular imaging analysis.

■ ASSOCIATED CONTENT

Supporting Information

The Supporting Information is available free of charge at https://pubs.acs.org/doi/10.1021/acs.analchem.3c01349.

Additional experimental details, materials, and methods, including photographs of the experimental setup (PDF)

Rotational movie of a rendered HeLa cell subjected to immunofluorescence staining with HSF4 (MP4)

■ AUTHOR INFORMATION

Corresponding Authors

Jun Ki Kim − *Asan Institute for Life Sciences, Asan Medical Center, Seoul 05505, Republic of Korea; Department of Biomedical Engineering, University of Ulsan College of Medicine, Seoul 05505, Republic of Korea;* orcid.org/0000-0002-0099-9681; Email: kim@amc.seoul.kr

Chan-Gi Pack − *Asan Institute for Life Sciences, Asan Medical Center, Seoul 05505, Republic of Korea; Department of Biomedical Engineering, University of Ulsan College of Medicine, Seoul 05505, Republic of Korea;* orcid.org/0000-0002-6578-3099; Email: changipack@amc.seoul.kr

Authors

Min Ju Cho − *Department of Medical Science, Asan Medical Institute of Convergence Science and Technology, Asan Medical Center, University of Ulsan College of Medicine, Seoul 05505, Republic of Korea*

Chae-Eun Kim − *Department of Medical Science, Asan Medical Institute of Convergence Science and Technology, Asan Medical Center, University of Ulsan College of Medicine, Seoul 05505, Republic of Korea*

Yeon Hui Shin − *Department of Medical Science, Asan Medical Institute of Convergence Science and Technology, Asan Medical Center, University of Ulsan College of Medicine, Seoul 05505, Republic of Korea*

Complete contact information is available at: https://pubs.acs.org/10.1021/acs.analchem.3c01349

Author Contributions

‖M.C. and C.-E.K. contributed equally to this work.

Notes

The authors declare no competing financial interest.

■ ACKNOWLEDGMENTS

We would like to thank Professor T. Yoshimori (Osaka University, Japan) for kindly providing HeLa cells stably expressing GFP-LC3 and Dr. T. K. Kim for his technical support. This work was supported by the National Research Foundation of Korea (NRF) (2019R1A2C2084122, 2018R1A5A2020732, and RS-2023-00238270), the Ministry of Science and ICT (MSIT), a grant from the Ministry of Trade, Industry, and Energy under the Industrial Technology Innovation Program (20000843), and the Korea Health Technology R&D Project through the Korea Health Industry Development Institute (KHIDI), funded by the Ministry of Health and Welfare, Republic of Korea (HI22C1374), and grants from the Asan Institute for Life Sciences, Asan Medical Center, Seoul, Korea (grant nos. 2021P0044-1, 2022IP0052-1, and 2023IP0071).

■ REFERENCES

(1) Lippincott-Schwartz, J.; Patterson, G. H. *Science* **2003**, *300*, 87−91.

(2) Pack, C.; Saito, K.; Tamura, M.; Kinjo, M. *Biophys. J.* **2006**, *91*, 3921−3936.

(3) Sako, Y.; Hiroshima, M.; Pack, C. G.; Okamoto, K.; Hibino, K.; Yamamoto, A. *Wiley Interdiscip. Rev.: Syst. Biol. Med.* **2012**, *4*, 183−192.

(4) Park, H.; Han, S. S.; Sako, Y.; Pack, C. G. *FASEB J.* **2015**, *29*, 837−848.

(5) Park, Y.; Depeursinge, C.; Popescu, G. *Nat. Photonics* **2018**, *12*, 578−589.

(6) Wolf, E. *Opt. Commun.* **1969**, *1*, 153−156.

(7) Park, Y. K.; Diez-Silva, M.; Popescu, G.; Lykotrafitis, G.; Choi, W.; Feld, M. S.; Suresh, S. *Proc. Natl. Acad. Sci. U.S.A.* **2008**, *105*, 13730−13735.

(8) Lim, J.; Ayoub, A. B.; Antoine, E. E.; Psaltis, D. *Light: Sci. Appl.* **2019**, *8*, 82.

(9) Jung, J.; Kim, K.; Yoon, J.; Park, Y. *Opt. Express* **2016**, *24*, 2006.

(10) Jung, J. H.; Hong, S. J.; Kim, H. B.; Kim, G.; Lee, M.; Shin, S.; Lee, S. Y.; Kim, D. J.; Lee, C. G.; Park, Y. K. *Sci. Rep.* **2018**, *8*, 6524.

(11) Kim, Y. S.; Lee, S.; Jung, J.; Shin, S.; Choi, H.-G.; Cha, G.-H.; Park, W.; Lee, S.; Park, Y. *Yale J. Biol. Med.* **2018**, *91*, 267−277.

(12) Kim, T. K.; Lee, B. W.; Fujii, F.; Kim, J. K.; Pack, C. G. *Cells* **2019**, *8*, 699.

(13) Kim, Y.; Kim, T. K.; Shin, Y.; Tak, E.; Song, G. W.; Oh, Y. M.; Kim, J. K.; Pack, C. G. *Mol. Cells* **2021**, *44*, 851−860.

(14) Kim, S. Y.; Lee, J. H.; Shin, Y.; Kim, T. K.; Lee, J. w.; Pyo, M. J.; Lee, A. R.; Pack, C. G.; Cho, Y. S. *Biochem. Biophys. Res. Commun.* **2022**, *587*, 42−48.

(15) Pack, C.-G. *Biophys. Physicobiol.* **2021**, *18*, 244−253.

(16) Yu, K. P.; Lee, G. W. M.; Lin, S. Y.; Huang, C. P. *J. Aerosol Sci.* **2008**, *39*, 377−392.

(17) Kim, K.; Park, W. S.; Na, S.; Kim, S.; Kim, T.; do Heo, W.; Park, Y. *Biomed. Opt. Express* **2017**, *8*, 5688.

(18) Jung, J. H.; Hong, S. J.; Kim, H. B.; Kim, G.; Lee, M.; Shin, S.; Lee, S. Y.; Kim, D. J.; Lee, C. G.; Park, Y. K. *Sci. Rep.* **2018**, *8*, 6524.

(19) Guo, R.; Barnea, I.; Shaked, N. T. *Biomed. Opt. Express* **2021**, *12*, 1869.

(20) Terasaki, M.; Loew, L.; Lippincott-Schwartz, J.; Zaal, K. *Current Protocols in Cell Biology*; Wiley, 2001; chapter 4, Unit 4.4.

(21) Su, J.-W.; Hsu, W.-C.; Tjiu, J.-W.; Chiang, C.-P.; Huang, C.-W.; Sung, K.-B. *J. Biomed. Opt.* **2014**, *19*, 075007.

(22) Baczewska, M.; Eder, K.; Ketelhut, S.; Kemper, B.; Kujawińska, M. *Cytometry, Part A* **2021**, *99*, 388−398.

(23) Kim, S. O.; Kim, J.; Okajima, T.; Cho, N. J. *Nano Convergence* **2017**, *4*, 5.

(24) Li, Y.; Almassalha, L. M.; Chandler, J. E.; Zhou, X.; Stypula-Cyrus, Y. E.; Hujsak, K. A.; Roth, E. W.; Bleher, R.; Subramanian, H.; Szleifer, I.; Dravid, V. P.; Backman, V. *Exp. Cell Res.* **2017**, *358*, 253−259.

(25) Fox, C. H.; Johnson, F. B.; Whiting, J.; Roller, P. P. *J. Histochem. Cytochem.* **1985**, *33*, 845−853.

(26) Hua, K.; Ferland, R. J. *Cilia* **2017**, *6*, 5.

(27) Kabeya, Y.; Mizushima, N.; Ueno, T.; Yamamoto, A.; Kirisako, T.; Noda, T.; Kominami, E.; Ohsumi, Y.; Yoshimori, T. *EMBO J.* **2000**, *19*, 5720−5728.
(28) Merath, K.; Ronchetti, A.; Sidjanin, D. *Invest. Ophthalmol. Vis. Sci.* **2013**, *54*, 6646−6654.
(29) Meder, V. S.; Boeglin, M.; de Murcia, G.; Schreiber, V. *J. Cell Sci.* **2005**, *118*, 211−222.
(30) Chen, D.; Huang, S. *J. Cell Biol.* **2001**, *153*, 169−176.
(31) Campbell, R. E.; Tour, O.; Palmer, A. E.; Steinbach, P. A.; Baird, G. S.; Zacharias, D. A.; Tsien, R. Y. *Proc. Natl. Acad. Sci. U.S.A.* **2002**, *99*, 7877−7882.
(32) Yasui, M.; Hiroshima, M.; Kozuka, J.; Sako, Y.; Ueda, M. *Nat. Commun.* **2018**, *9*, 3061.
(33) Park, Y.; Diez-Silva, M.; Fu, D.; Popescu, G.; Choi, W.; Barman, I.; Suresh, S.; Feld, M. S. *J. Biomed. Opt.* **2010**, *15*, 020506.
(34) Kim, G.; Lee, M.; Youn, S. Y.; Lee, E. T.; Kwon, D.; Shin, J.; Lee, S. Y.; Lee, Y. S.; Park, Y. K. *Sci. Rep.* **2018**, *8*, 9192.
(35) Kim, T. K.; Lee, B. W.; Fujii, F.; Lee, K. H.; Lee, S.; Park, Y.; Kim, J. K.; Lee, S. W.; Pack, C. G. *Cells* **2019**, *8*, 1368.
(36) Debnath, S. K.; Park, Y. *Opt. Lett.* **2011**, *36*, 4677.
(37) Takeda, M.; Ina, H.; Kobayashi, S. *JOSA* **1982**, *72*, 156−160.
(38) Bandyopadhyay, D.; Cyphersmith, A.; Zapata, J. A.; Kim, Y. J.; Payne, C. K. *PLoS One* **2014**, *9*, No. e86847.
(39) Targett-Adams, P.; Chambers, D.; Gledhill, S.; Hope, R. G.; Coy, J. F.; Girod, A.; McLauchlan, J. *J. Biol. Chem.* **2003**, *278*, 15998−16007.
(40) Cheng, R.; Zhang, F.; Li, M.; Wo, X.; Su, Y. W.; Wang, W. *Front. Chem.* **2019**, *7*, 588.
(41) Reisler, E.; Eisenberg, H.; Minton, A. P. *J. Chem. Soc., Faraday Trans. 2* **1972**, *68*, 1001−1015.
(42) Khodier, S. A. *Opt. Laser Technol.* **2002**, *34*, 125−128.
(43) Jiao, X.; Khan, S. Y.; Kaul, H.; Butt, T.; Naeem, M. A.; Riazuddin, S.; Hejtmancik, J. F.; Riazuddin, S. A. *PLoS One* **2019**, *14*, No. e0225010.
(44) Huang, S.; Xu, X.; Wang, G.; Lu, G.; Xie, W.; Tao, W.; Zhang, H.; Jiang, Q.; Zhang, C. *J. Cell Sci.* **2016**, *129*, 1429−1440.
(45) Finch, R. A.; Revankar, G. R.; Chan, P. K. *J. Biol. Chem.* **1993**, *268*, 5823−5827.
(46) Kumar, P.; Nagarajan, A.; Uchil, P. D. *Cold Spring Harb. Protoc.* **2019**, *2019*, 681−683.
(47) Hawley-Nelson, P.; Ciccarone, V.; Moore, M. L. *Current Protocols in Molecular Biology*; Wiley, 2008; chapter 9, unit 9.4.
(48) Fus-Kujawa, A.; Prus, P.; Bajdak-Rusinek, K.; Teper, P.; Gawron, K.; Kowalczuk, A.; Sieron, A. L. *Front. Bioeng. Biotechnol.* **2021**, *9*, 701031.
(49) Shimi, T.; Pfleghaar, K.; Kojima, S. I.; Pack, C. G.; Solovei, I.; Goldman, A. E.; Adam, S. A.; Shumaker, D. K.; Kinjo, M.; Cremer, T.; Goldman, R. D. *Genes Dev.* **2008**, *22*, 3409−3421.
(50) Tanaka, T.; Zhou, Y.; Ozawa, T.; Okizono, R.; Banba, A.; Yamamura, T.; Oga, E.; Muraguchi, A.; Sakurai, H. *J. Biol. Chem.* **2018**, *293*, 2288−2301.
(51) Terasaki, M.; Loew, L.; Lippincott-Schwartz, J.; Zaal, K. *Current Protocols in Cell Biology*; Wiley, 2001; chapter 4 (1), unit 4.4.
(52) Ren, W.; Wang, D.; Huang, W.; Li, J.; Tian, X.; Liu, Z.; Han, G.; Liu, B.; Han, M. Y.; Zhang, Z.; Zhang, R. *Dyes Pigm.* **2021**, *191*, 109366.
(53) Bucevičius, J.; Lukinavičius, G.; Gerasimaite, R. *Chemosensors* **2018**, *6*, 18.
(54) Kabeya, Y.; Mizushima, N.; Ueno, T.; Yamamoto, A.; Kirisako, T.; Noda, T.; Kominami, E.; Ohsumi, Y.; Yoshimori, T. *EMBO J.* **2000**, *19*, 5720−5728.
(55) Ni, H. M.; Bockus, A.; Wozniak, A. L.; Jones, K.; Weinman, S.; Yin, X. M.; Ding, W. X. *Autophagy* **2011**, *7*, 188−204.
(56) Kaizuka, T.; Morishita, H.; Hama, Y.; Tsukamoto, S.; Matsui, T.; Toyota, Y.; Kodama, A.; Ishihara, T.; Mizushima, T.; Mizushima, N. *Mol. Cell* **2016**, *64*, 835−849.
(57) Baumann, O.; Walz, B. *Int. Rev. Cytol.* **2001**, *205*, 149−214.
(58) Voeltz, G. K.; Prinz, W. A.; Shibata, Y.; Rist, J. M.; Rapoport, T. A. *Cell* **2006**, *124*, 573−586.
(59) Kim, K.; Lee, S.; Yoon, J.; Heo, J.; Choi, C.; Park, Y. *Sci. Rep.* **2016**, *6*, 36815.
(60) Ni, H. M.; Bockus, A.; Wozniak, A. L.; Jones, K.; Weinman, S.; Yin, X. M.; Ding, W. X. *Autophagy* **2011**, *7*, 188−204.

https://doi.org/10.1021/acs.analchem.3c01349
Anal. Chem. 2023, 95, 13478−13487